A cantilever-free approach to dot-matrix nanoprinting

Keith A. Brown[a,b], Daniel J. Eichelsdoerfer[a,b], Wooyoung Shim[b,c], Boris Rasin[b,c], Boya Radha[a,b], Xing Liao[b,c], Abrin L. Schmucker[a,b], Guoliang Liu[a,b], and Chad A. Mirkin[a,b,c,1]

Departments of [a]Chemistry and [c]Materials Science and Engineering and [b]International Institute for Nanotechnology, Northwestern University, Evanston, IL 60208

Contributed by Chad A. Mirkin, June 26, 2013 (sent for review May 25, 2013)

Scanning probe lithography (SPL) is a promising candidate approach for desktop nanofabrication, but trade-offs in throughput, cost, and resolution have limited its application. The recent development of cantilever-free scanning probe arrays has allowed researchers to define nanoscale patterns in a low-cost and high-resolution format, but with the limitation that these are duplication tools where each probe in the array creates a copy of a single pattern. Here, we report a cantilever-free SPL architecture that can generate 100 nanometer-scale molecular features using a 2D array of independently actuated probes. To physically actuate a probe, local heating is used to thermally expand the elastomeric film beneath a single probe, bringing it into contact with the patterning surface. Not only is this architecture simple and scalable, but it addresses fundamental limitations of 2D SPL by allowing one to compensate for unavoidable imperfections in the system. This cantilever-free dot-matrix nanoprinting will enable the construction of surfaces with chemical functionality that is tuned across the nano- and macroscales.

nanofabrication | polymer pen lithography | thermal actuation | soft microelectromechanical systems

Throughout the last century, printing tools have been transformed from large instruments at remote sites to low-cost point-of-use ones. In contrast, integrated circuits are mass-produced using a limited set of materials at centralized facilities (1). To accommodate emerging applications in nanotechnology, materials science, and biotechnology, lithographic tools must be made materials-general and moved from the cleanroom to the desktop (2, 3). Methods of scanning probe lithography (SPL), such as dip-pen nanolithography (4–6), compare favorably to alternatives such as inkjet printing (7, 8) from a resolution and scalability standpoint (4, 9–11), but throughput is a critical limitation. Although it is conceivable that cantilever-based tools could one day be widely applied for SPL—in fact, impressive advances have been made in the development of actuated (11–16) and high-density (17) cantilever arrays—the high cost and fragility of these systems have prevented their widespread use (18). In contrast, arrays of pens in a cantilever-free architecture point toward a viable solution for rapidly making high-resolution patterns of materials at low cost (19–23); however, these techniques currently lack the flexibility to make patterns independently with each tip in an array. These techniques, such as polymer pen lithography (PPL) (19), will not be widely used unless simple and scalable methods of incorporating independent actuation are developed. Previous attempts to address this by actuating individual pens have used pneumatic actuation and thus failed to provide an architecture that allows massive parallelization (13, 14).

Herein, we describe an architecture and patterning methodology that together allow one to actuate individual pens in a cantilever-free pen array and print arbitrary nanoscale arrangements of molecules across large scales while compensating for the nonidealities of individual pens. A passive cantilever-free SPL system consists of an array of pens resting on a compliant polydimethylsiloxane (PDMS) film on a rigid glass slide to maintain array planarity. However, for each pen in the array to print materials independently, they must be actuated micrometer distances relative to one another. The actuated cantilever-free architecture described herein involves fabricating a resistive heater directly below each elastomeric pen in a PPL array (Fig. 1) and relies on the hypothesis that heat can be used to expand the PDMS in such a way that one can reliably actuate the pens without significant cross-talk or degradation in performance. This simple approach is promising from a scalability perspective, because electrical heaters can be readily fabricated as planar devices on the glass layer and can easily be electrically addressed in a multiplexed fashion. Furthermore, PDMS is an optimal material for thermal actuation because of its high coefficient of thermal expansion (24, 25) and thermal stability (26).

Results and Discussion

The proof-of-concept active PPL architecture used here consists of a 150-μm pitch, 4 × 4 array of heaters fabricated out of indium tin oxide on a glass slide that was subsequently coated with a PDMS film (*Materials and Methods* and Fig. S1). To evaluate this actuation scheme, an atomic force microscope (AFM) was used to visualize the motion of the surface when locally heated (Fig. 2*A*). In a typical experiment, a heater was periodically driven with a power P, resulting in a series of heating and cooling trajectories as measured by AFM (Fig. 2*B*). Fitting the heating trajectory to a biexponential function provided a measure of the average rise time τ and maximum actuation amplitude A, for a given P. From this experiment with $P = 40$ mW, A and τ were found to be 4.185 ± 0.005 μm and 36.12 ± 0.06 ms, respectively. Additional experiments revealed that A varied linearly with P (Fig. 2*C*), a result consistent with a lumped element model (*SI Text* and Figs. S2 and S3) in which the experimentally determined 107 ± 2 nm/mW slope of A vs. P represents the actuation efficiency and is in agreement with the 110 nm/mW efficiency predicted by theory (27, 28). Here, τ has a mean value of 39 ms, in agreement with the predicted value of 41 ms, and its gentle variation with P is attributed to temperature-dependent material properties. Additionally, repeating this experiment with the AFM tip positioned at different distances along the surface of the PDMS (Fig. 2*D*) revealed that this actuation scheme has acceptable levels of crosstalk and fatigue for effective actuation (*SI Text* and Fig. S4).

Having observed that thermal actuation meets the criteria for actuating pens in a cantilever-free array, we considered the challenges associated with multiplexed SPL-based molecular printing. Ideally, every pen in the array would be the same distance from a surface such that the actuation of any given pen brings it into contact with the surface. Practically, there are three effects that prevent this from being the case (Fig. S5). (*i*) The pen array may not be coplanar with the surface. This issue has been resolved in cantilever-free SPL with force (29) or optical (19) leveling procedures; here, all components are transparent, and thus optical leveling was used. (*ii*) Once the pen array and patterning surface

Author contributions: K.A.B., W.S., and C.A.M. designed research; K.A.B., D.J.E., W.S., B. Rasin, B. Radha, X.L., A.L.S., and G.L. performed research; K.A.B., D.J.E., W.S., B. Rasin, B. Radha, X.L., A.L.S., and G.L. analyzed data; and K.A.B., D.J.E., W.S., B. Rasin, B. Radha, X.L., A.L.S., G.L., and C.A.M. wrote the paper.

The authors declare no conflict of interest.

[1]To whom correspondence should be addressed. E-mail: chadnano@northwestern.edu.

This article contains supporting information online at www.pnas.org/lookup/suppl/doi:10.1073/pnas.1311994110/-/DCSupplemental.

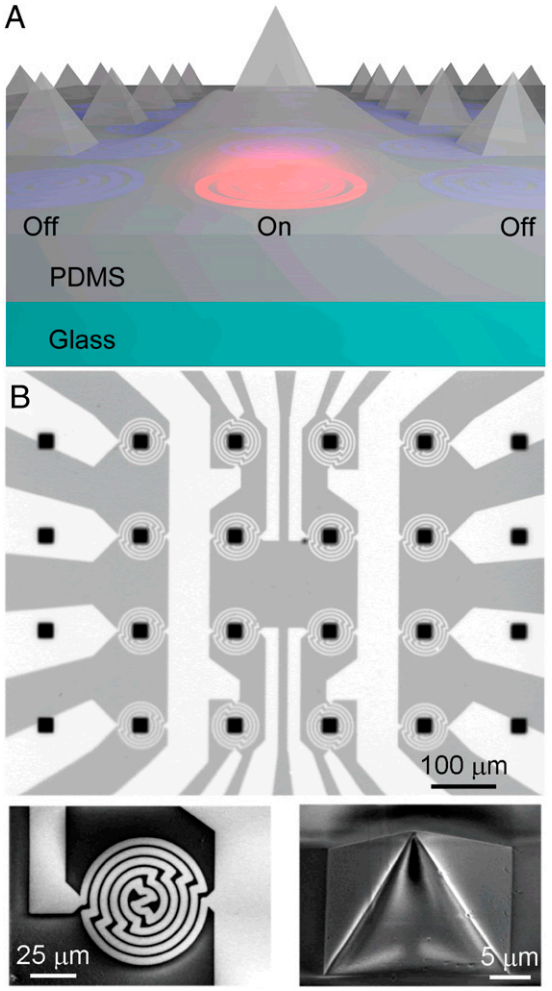

Fig. 1. Active PPL. (*A*) Schematic of an active PPL pen array in which a resistive heater is positioned below each pen. In this schematic, the center pen is actuated by the thermal expansion of the PDMS. (*B*) Optical micrograph of a 4 × 4 array of active PPL pens coupled with heaters. (*Lower*) SEM images of a bare heater coil (*Left*) and an individual PDMS pen (*Right*).

are coplanar, they are not necessarily coplanar with the horizontal motion of the stage, resulting in the tip-sample height varying with the *x*–*y* position of the sample. (*iii*) Finally, variations in the height of individual pens or the performance of actuators will result in differences in printing. Whereas issues *ii* and *iii* are unavoidable in any 2D SPL system, if they can be measured, they can be compensated for. To our knowledge, these critical issues have never been discussed in the context of 2D SPL.

To probe the aforementioned challenges and prospects for overcoming them, proof-of-concept active PPL patterning experiments were conducted. An active PPL array was silver-epoxied to a printed circuit board, drop-coated with 5 mM 16-mercaptohexadecanoic acid (MHA) in acetonitrile, and mounted in a SPL instrument (*SI Text* and Fig. S6). The pen array was then optically leveled with respect to a Au-coated Si wafer chip, addressing issue *i*. To determine the importance of issue *ii*, we recorded the tip-sample separation at each of the four corners of the patterning canvas. Typically, the tip-sample separation varied ∼2 μm across the 150 × 150 μm^2 patterning region, representing a significant enough variation to interfere with patterning. To compensate for this effect, these four points were fit to a plane that was used to interpolate the estimated tip-sample separation at any location. By positioning the tip array within this plane, we ensured that the tip array was at a specified distance from the surface, thus addressing issue *ii*.

Having determined a procedure for maintaining a well-defined tip-sample separation at all locations on the patterning canvas, we performed a preliminary patterning experiment. In this experiment, the pen array visited a 5 × 5 array of points where at each location each pen was sequentially actuated with 8.3 mW for 500 ms at 60% relative humidity (RH). Custom electronics and software were used to operate the heater array in synchrony with the operation of the SPL instrument (*SI Text*, Fig. S7, and Movie S1). In this and all patterning experiments, MHA features were written on Au-coated Si substrates and subsequently used as etch masks for a Au etchant, allowing the molecular patterns to be visualized as Au regions. SEM revealed that each pen wrote a uniform array

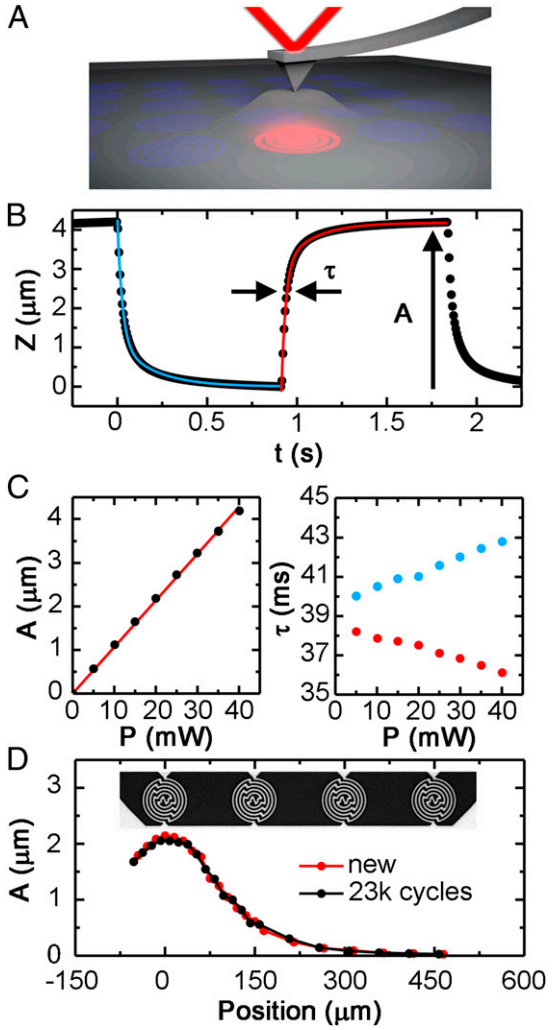

Fig. 2. Characterization of thermal actuation. (*A*) The experimental setup, consisting of an AFM probe measuring the expansion of a PDMS film above an activated heater. (*B*) The vertical trajectory Z of the AFM probe, where periodic actuation of the heater is observed as an overdamped square wave. The amplitude *A* and rise time τ of this measured actuation were estimated from fits to the heating (red) and cooling (blue) curves. (*C*) Varying the applied power *P* resulted in a linear variation in *A* and a small variation in τ measured for heating (red) and cooling (blue). (*D*) By moving the AFM probe along the surface of the heater array, the spatial profile of actuation was measured. The red curve shows the initially measured profile and the black curve is from the same measurement repeated after 12 h of continuous cycling. An SEM image of four heater coils is shown to scale with the abscissa to illustrate the magnitude of cross-talk between heaters.

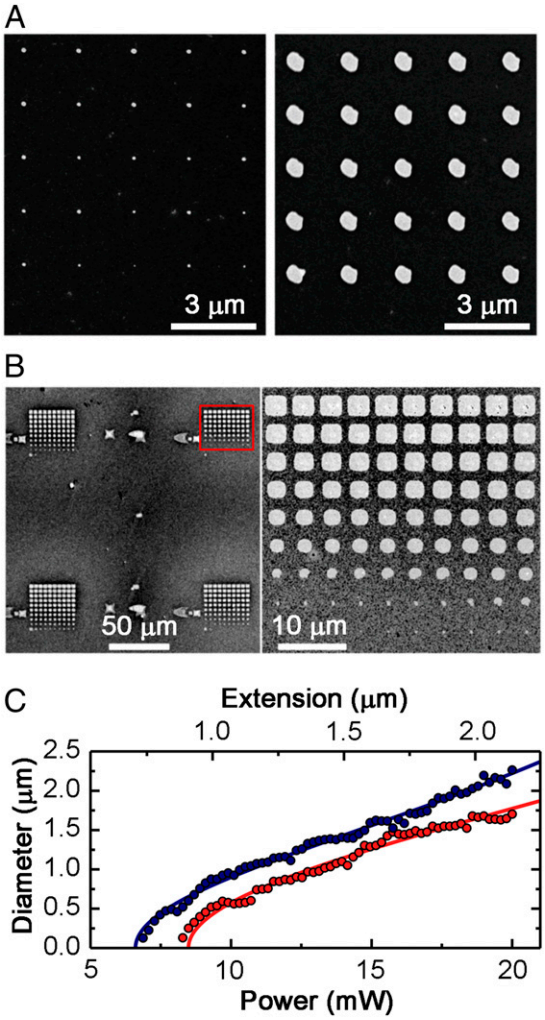

Fig. 3. Power dependence and active pen calibration. (*A*) SEM image of 5 × 5 dot features written by two pens each with 8.3 mW of applied power. (*B*) SEM image of gold features patterned by four pens in an active PPL pen array. (*Right*) A magnified view of the area highlighted in red. In each dot array, the applied power increases continuously from 0 on the bottom left to 32 mW at the top right. (*C*) The diameter of features written by two pens vs. applied power and calculated actuation distance. Solid lines are inverse Lorentzian fits to the data.

of points, with the features written by two pens shown in Fig. 3*A*. This experiment also revealed that features with an average diameter of 125 ± 33 nm were written and that larger features, such as those with an average diameter of 659 ± 13 nm, were written with much lower variance in size, a phenomenon that is explored further below. These observations also signify that, without calibration, different pens will generate features of different sizes.

To explore the relationship between actuation strength and the resulting printed feature size, an actuation sweep experiment was performed. In this experiment, the pen array visited a 10 × 10 array of points, and at each point each pen was actuated for 2 s with a power that was swept from 0 to 32 mW. SEM imaging showed that each tip wrote an array of features of varying size, ranging from small features at low power to large features at high power (Fig. 3*B*). Note that smaller features were round on account of their diffusion-limited character, whereas larger features were square, reflecting their formation through stamping, due to the deformable nature of the PDMS tips (19). In a subsequent actuation sweep experiment in which *P* was varied from 0 to 20 mW, the diameters of the features written by two pens were measured (Fig. 3*C*). Although both patterns exhibited a smooth and monotonic dependence of feature diameter on applied power, the minimum power at which features were generated differed. This effect is attributed to a ∼200 nm estimated variation in height between the pens. For both pens, feature size vs. power fit very well to the inverse of a Lorentzian with an offset (solid lines in Fig. 3*C*). Interestingly, the decreasing slope of feature diameter vs. extension explains why larger features exhibit less variance in average size. By allowing one to compute the power required for a given pen to write a feature of a given size, this calibration accounts for nonidealities in pens and actuators, thus addressing challenge *iii*. Importantly, once done for a given pen array, this calibration need not be done again. Indeed, we did not observe any loss of calibration for a given pen array over the course of 10 sequential patterning experiments. However, the ability to dial in a given feature size is dependent upon how accurately the tip-sample separation is determined. Here, we used an optical scheme that provided ∼200 nm resolution. To improve on this, one can use a force-based method to precisely determine tip-sample separation (29) or use hard tips where the printed feature size is invariant of contact force (20). It is worth emphasizing that whereas uncertainty in tip-sample distance is what currently limits the resolution of active PPL, very finely spaced actuation sweep experiments were used to print sub-50-nm features at a pitch of 100 nm (*SI Text* and Fig. S8).

After developing a methodology to overcome the three patterning challenges listed above, we performed an experiment to evaluate the ability of active PPL to print highly uniform arrays of molecular features wherein each pen is actuated independently. Active PPL was used to print a 600 × 600 μm^2 image of a portion of the periodic table of elements that consisted of 5,961 features written as the tip array visited 1,192 unique positions (Fig. 4). Here, each tip patterned the region corresponding to a different element. The average feature size was determined to be 1.28 ± 0.04 μm. To maintain feature-size uniformity across the array, the power applied to each pen was calibrated by selecting a power from an actuation sweep experiment that corresponded to the same feature size. This patterning experiment was performed using an actuation time of 200 ms at 20% RH with a pen-specific power between 20 and 32 mW.

Taken together, this work demonstrates a cantilever-free printing tool capable of arbitrary pattern generation across multiple tips with high resolution. This tool combines the flexibility of an inkjet printer with the ability to generate 100-nm-scale

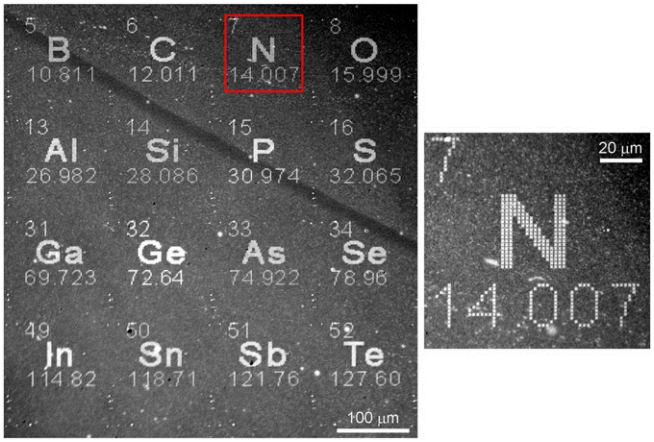

Fig. 4. Arbitrary patterning with active PPL. Optical micrograph of a portion of the periodic table of the elements patterned by a 4 × 4 active PPL pen array. (*Inset*) A magnified view of the "nitrogen" entry written by a single pen.

features, while maintaining the simplicity and low cost of the cantilever-free architecture. Although a 4×4 array was explored as a proof-of-concept, given the fact that PPL pen arrays with up to 11 million pens have been reported (19) and that with appropriate engineering it is possible to electrically multiplex millions of electrical circuits, it is reasonable to project that this technique can be expanded to thousands or millions of pens. Indeed, by providing approaches to address key issues in pattern versatility and quality, this lowers some of the greatest barriers to transitioning the field of SPL from one of academic curiosity to one that can be centered on point-of-use prototyping or production capabilities.

Materials and Methods

Active Heater Fabrication. The steps of active PPL pen array fabrication are outlined in Fig. S1. Transparent heater arrays were fabricated by etching 25×25 mm^2 glass slides coated in 8–12 Ω/sq indium tin oxide (ITO) (703192; Sigma-Aldrich). Heater coil patterns were photolithographically defined with a positive tone photoresist (S1818; Shipley). To make the patterns more resistant to dry etching, samples were hard-baked in an oven overnight at 80 °C. To etch the ITO, samples were etched under a 5-mTorr atmosphere with 200 sccm Ar, 2,500 W RF power, and 80 W delivered to the platen in a deep reactive ion etch tool (STS LpX Pegasus) (30). Under these conditions, the etch rate of ITO was found to be ∼1 Å/s. The completion of this etch was verified by using a multimeter to measure the resistance of the heater coils. Residual resist was removed using an overnight soak in Remover PG (Microchem) on a hot plate at 80 °C, and the final heater coils were visualized in a SEM (Fig. 1*B*). Arrays of square pyramidal holes that form masters for PPL pens were fabricated out of 4-inch Si <100> wafers (Nova Electronic Materials) according to a literature protocol (19). A PPL master was then spin-coated with 10:1 base:cross-linker PDMS (Sylgad 184; Dow Corning) at 1,000 rpm for 30 s and subsequently covered with a heater array, taking care to avoid trapped bubbles. This process resulted in PDMS films that were 90 ± 2 μm thick. To align the PPL pens with the heaters, the structure was placed on a hot plate in view of an optical microscope. The heater array was manipulated until the alignment between the PPL pens and the heater was better than 3 μm. At this point, the hot plate was turned on for ∼3 min until the heater array could no longer slide freely, setting the alignment. The structure was then cured in an oven at 80 °C overnight. When the active PPL pen array was peeled off the master, the PDMS over the contact pads was stripped with a blade and a stylus profilometer was used to measure the thickness of the PDMS film (Dektak-8; Veeco Instruments).

Characterization of Thermal Actuation. Thermal actuation was measured using a commercial AFM (Dimension Icon; Bruker). For characterization purposes, samples consisting of the heater coil array and PDMS coating layer without a tip array were used (Fig. 2*A*). Data were acquired by scanning in contact mode using a contact mode probe (PPP-CONT; NanoWorld AG) in a 100×100 nm^2 region on the PDMS above the heater. Ten line scans were taken with a resolution of 4,096 points per line at 0.1 Hz. The deflection set point was 1 V and the integral and proportional gains were 5 and 10, respectively. At the same time, a specified heater was driven with a 0.5-Hz square wave at a set power P that was determined by measuring the applied voltage and current. The height recorded by the AFM was an overdamped square wave where the damping is caused by the finite heating time of the PDMS (Fig. 2*B*). Each rise and fall of the height was fit to the sum of two exponentials and characterized by the total amplitude A and a rise time τ defined to be the time required to reach 63% of the maximum value—a measure that for a single rising exponential function would recover the time constant of that exponential. At each applied power, the average A and τ were found from all 10 lines of the saved AFM image. The SDs in A and τ were also calculated, but they are much smaller than the points in Fig. 2 *C* and *D*.

Patterning with Active PPL. Before leveling, the tip arrays were inked with a 5 mM solution of MHA (Sigma-Aldrich) dissolved in acetonitrile. The inking procedure entailed plasma-cleaning the tip array in a 10-W air plasma for 2 min at 200 mTorr, drop-casting 25 μL of ink solution onto the tip array, and allowing the ink to dry under ambient conditions. Si <100> wafers (Nova Electronic Materials) for patterning were coated with 5 nm of Cr and 25 nm of Au in an electron beam evaporation system (Kurt J. Lesker Company). Patterning was performed in a customized commercial scanning probe instrument (XE-150; Park Systems) in a temperature- and humidity-controlled environment. RH was not observed to be a critical factor, with patterning at RH between 20% and 60% resulting in comparable patterns. Samples were diced into ∼1-cm^2 chips for patterning and used within a week of deposition. After patterning, samples were etched for ∼5 min in an $Fe(NO_3)_3$/thiourea/HCl etchant (consisting of aqueous solutions of 27 mM $Fe(NO_3)_3$, 40 mM thiourea, and 100 mM HCl mixed in equal parts by volume) and visualized by optical microscopy (Axiovert 200M; Zeiss) and scanning electron microscopy (S-4800-II; Hitachi).

ACKNOWLEDGMENTS. This work was supported by US Air Force Office of Scientific Research (AFOSR) Awards FA9550-12-1-0280 and FA9550-12-1-0141, Defense Advanced Research Projects Agency Award N66001-08-1-2044, and National Science Foundation Awards DBI-1152139 and DMB-1124131 (to C.AM.). K.A.B. and X.L. gratefully acknowledge support from Northwestern University's International Institute for Nanotechnology. D.J.E. acknowledges the Department of Defense and AFOSR for National Defense Science and Engineering Graduate Fellowship 32 CFR 168a. B. Radha acknowledges the Indo–US Science and Technology Forum for a postdoctoral fellowship.

1. Peercy PS (2000) The drive to miniaturization. *Nature* 406(6799):1023–1026.
2. Hertzberg RP, Pope AJ (2000) High-throughput screening: New technology for the 21st century. *Curr Opin Chem Biol* 4(4):445–451.
3. Gratton SEA, et al. (2008) The pursuit of a scalable nanofabrication platform for use in material and life science applications. *Acc Chem Res* 41(12):1685–1695.
4. Piner RD, Zhu J, Xu F, Hong S, Mirkin CA (1999) "Dip-pen" nanolithography. *Science* 283(5402):661–663.
5. Ginger DS, Zhang H, Mirkin CA (2004) The evolution of dip-pen nanolithography. *Angew Chem Int Ed* 43(1):30–45.
6. Salaita K, Wang Y, Mirkin CA (2007) Applications of dip-pen nanolithography. *Nature Nanotech* 2(3):145–155.
7. Park J-U, et al. (2007) High-resolution electrohydrodynamic jet printing. *Nature Mater* 6(10):782–789.
8. Ahn BY, et al. (2009) Omnidirectional printing of flexible, stretchable, and spanning silver microelectrodes. *Science* 323(5921):1590–1593.
9. Kim Y, Lieber CM (1992) Machining oxide thin films with an atomic force microscope: Pattern and object formation on the nanometer scale. *Science* 257(5068):375–377.
10. Betzig E, Trautman JK (1992) Near-field optics: Microscopy, spectroscopy, and surface modification beyond the diffraction limit. *Science* 257(5067):189–195.
11. Vettiger P, et al. (2000) The "Millipede"— More than one thousand tips for future AFM data storage. *IBM J Res Develop* 44(3):323–340.
12. Wang X, Bullen DA, Zou J, Liu C, Mirkin CA (2004) Thermally actuated probe array for parallel dip-pen nanolithography. *J Vac Sci Technol B* 22(6):2563–2567.
13. Li S, Dellinger TM, Wang Q, Szegedi S, Liu C (2007) Pneumatically actuated elastomeric device for nanoscale surface patterning. *Appl Phys Lett* 91(2):023109-1–023109-3.
14. Han Y, Liu C (2011) Pneumatically actuated active polymer pen lithography. *Sens Actuators A Phys* 167:433–437.
15. Bullen D, et al. (2004) Parallel dip-pen nanolithography with arrays of individually addressable cantilevers. *Appl Phys Lett* 84(5):789–791.
16. Bullen D, Liu C (2006) Electrostatically actuated dip pen nanolithography probe arrays. *Sens Actuators A Phys* 125:504–511.
17. Salaita K, et al. (2006) Massively parallel dip-pen nanolithography with 55 000-pen two-dimensional arrays. *Angew Chem Int Ed* 45(43):7220–7223.
18. Tseng AA, Notargiacomo A, Chen TP (2005) Nanofabrication by scanning probe microscope lithography: A review. *J Vac Sci Technol B* 23(3):877–894.
19. Huo F, et al. (2008) Polymer pen lithography. *Science* 321(5896):1658–1660.
20. Shim W, et al. (2011) Hard-tip, soft-spring lithography. *Nature* 469(7331):516–520.
21. Xie Z, et al. (2012) Polymer pen lithography using dual-elastomer tip arrays. *Small* 8(17):2664–2669.
22. Shim W, et al. (2012) Multifunctional cantilever-free scanning probe arrays coated with multilayer graphene. *Proc Natl Acad Sci USA* 109(45):18312–18317.
23. Eichelsdoerfer DJ, Brown KA, Boya R, Shim W, Mirkin CA (2013) Tuning the spring constant of cantilever-free tip arrays. *Nano Lett* 13(2):664–667.
24. Grzybowski BA, Brittain ST, Whitesides GM (1999) Thermally actuated interferometric sensors based on the thermal expansion of transparent elastomeric media. *Rev Sci Instrum* 70(4):2031–2037.
25. Sz-Yuan L, Hsi-Wen T, Wen-Chih C, Weileun F (2006) Thermal actuated solid tunable lens. *IEEE Photon Technol Lett* 18(21):2191–2193.
26. Camino G, Lomakin SM, Lazzari M (2001) Polydimethylsiloxane thermal degradation Part 1. Kinetic aspects. *Polymer* 42(6):2395–2402.
27. Mark J (1999) *Polymer Data Handbook* (Oxford Univ Press, New York).
28. Haynes WM, ed (2012) *CRC Handbook of Chemistry and Physics* (CRC, Boca Raton, FL), 93rd Ed.
29. Liao X, Braunschweig AB, Mirkin CA (2010) "Force-feedback" leveling of massively parallel arrays in polymer pen lithography. *Nano Lett* 10(4):1335–1340.
30. Saia RJ, Kwasnick RF, Wei CY (1991) Selective reactive ion etching of indium-tin oxide in a hydrocarbon gas mixture. *J Electrochem Soc* 138(2):493–496.